Enhanced Fibrinolysis with Magnetically Powered Colloidal Microwheels

Tonguc O. Tasci, Dante Disharoon, Rogier M. Schoeman, Kuldeepsinh Rana, Paco S. Herson, David W. M. Marr, and Keith B. Neeves**

***T**hrombi that occlude blood vessels can be resolved with fibrinolytic agents that degrade fibrin, the polymer that forms between and around platelets to provide mechanical stability. Fibrinolysis rates however are often constrained by transport-limited delivery to and penetration of fibrinolytics into the thrombus. Here, these limitations are overcome with colloidal microwheel (μwheel) assemblies functionalized with the fibrinolytic tissue-type plasminogen activator (tPA) that assemble, rotate, translate, and eventually disassemble via applied magnetic fields. These microwheels lead to rapid fibrinolysis by delivering a high local concentration of tPA to induce surface lysis and, by taking advantage of corkscrew motion, mechanically penetrating into fibrin gels and platelet-rich thrombi to initiate bulk degradation. Fibrinolysis of plasma-derived fibrin gels by tPA-microwheels is fivefold faster than with 1 μg mL^{-1} tPA. μWheels following corkscrew trajectories can also penetrate through 100 μm sized platelet-rich thrombi formed in a microfluidic model of hemostasis in ≈5 min. This unique combination of surface and bulk dissolution mechanisms with mechanical action yields a targeted fibrinolysis strategy that could be significantly faster than approaches relying on diffusion alone, making it well-suited for occlusions in small or penetrating vessels not accessible to catheter-based removal.*

Dr. T. O. Tasci, D. Disharoon, Dr. R. M. Schoeman, Dr. K. Rana, Prof. D. W. M. Marr, Prof. K. B. Neeves
Chemical and Biological Engineering Department
Colorado School of Mines
1500 Illinois St., Golden, CO 80401, USA
E-mail: dmarr@mines.edu; kneeves@mines.edu

Prof. P. S. Herson
Department of Anesthesiology
University of Colorado School of Medicine
12800 East 19th Ave., Aurora, CO 80045, USA

Prof. P. S. Herson
Department of Pharmacology
University of Colorado School of Medicine
12800 East 19th Ave., Aurora, CO 80045, USA

Prof. K. B. Neeves
Department of Pediatrics
University of Colorado School of Medicine
12800 East 19th Ave., Aurora, CO 80045, USA

The ORCID identification number(s) for the author(s) of this article can be found under https://doi.org/10.1002/smll.201700954.

DOI: 10.1002/smll.201700954

1. Introduction

Biochemical dissolution of blood clots, or thrombi, involves systemic or local delivery of plasminogen activators (PA) such as tissue-type plasminogen activator (tPA) and urokinase.[1] These PA convert plasminogen to plasmin, which in turn lyses fibrin fibers, the biopolymer that provides thrombi mechanical stability.[2] The efficacy of fibrinolytic therapy is limited by two transport barriers, the rate of delivery of PA to an occlusive thrombus, and the rate of dissolution. Delivery rates depend on the thrombus location and mode of administration; for example, during intravenous administration the concentration of PA is limited by diffusion to the occlusive thrombi interface when residual blood flow is minimal.[3] The rate of diffusion can be increased with higher systemic concentration, but values are limited by inherent bleeding risks associated with fibrinolytic therapy.[4] For catheter-based delivery, the local concentration can be higher than systemic administration; however, this delivery approach is limited to accessible large arteries. While dissolution rates generally

depend on the local PA concentration, the thrombus composition, and the pressure gradient across the thrombus,[5] in most cases removal is limited by PA penetration rather than by the kinetics of fibrin degradation.[6] This combined restriction of transport of drug to and through the thrombus can significantly limit the time to reperfusion using biochemical methods alone.

Drug delivery via PA-functionalized micro- and nanoparticles or blood cells is an alternative approach that can result in higher local concentrations and faster lysis than systemic administration of PA alone.[7–9] When coupled with moieties that recognize fibrin(ogen) or transmembrane proteins on platelets,[10] such particles can enhance accumulation at the surface of thrombi or take advantage of the unique fluid dynamics of a stenosed vessel.[9] These approaches however rely on blood flow to deliver particles to the injury site, which requires particles in circulation prior to what is typically an acute and unpredictable thrombotic event. As a result, there is a need for drug delivery strategies that can bring high concentrations of fibrinolytics to the surface of thrombi that does not rely on blood flow or diffusion alone. This is especially critical for occlusions present in vessels not accessible to catheters including deep penetrating cerebral arteries that are sites for lacunar strokes.[11] To deliver PA down such blocked vessels requires an alternative driving force, one that is not dependent on concentration or pressure gradients and yet is rapid enough to function within therapeutic time scales. Electromagnetic field-based approaches are such an alternative and others have used magnetic field gradients to drive PA immobilized on magnetic particles to a thrombus surface;[12–15] however, the field gradients required for rapid translation by magnetophoresis are quite high ($\approx$1 T m^{-1}) and difficult and expensive to implement in a clinical setting. Other field-based approaches to overcome diffusion limitations include enhancing mixing to reduce concentration gradients at the thrombus interface[16] or enhancing fibrinolysis with mechanical forces induced by ultrasound.[17,18] However, the attenuation of ultrasound in tissues limits its use to superficial or easily accessible vessels.

To address these issues and without employing field gradients, we recently reported the assembly and translation of magnetically powered colloidal microwheels (μwheels) capable of translation at speeds of over 100 μm s^{-1}.[19] In this, superparamagnetic microparticles cluster into wheel-like shapes when subject to a low-strength planar rotating magnetic field.[20,21] Here, the rotation of the field induces a torque that, when balanced by fluid drag, leads to wheel rotation that depends on field frequency.[22,23] In these studies, we have shown that, by orienting the field in a normal fashion and exploiting friction between μwheels and adjacent surfaces, significant μwheel translation speeds can be achieved. Travel direction can be precisely, rapidly, and readily controlled by simply shifting the applied field phase angle making control both immediate and precise. With both assembly and translation manipulated via weak, order milliTesla, external magnetic fields that do not attenuate in tissue, this method could be well-suited as a drug delivery strategy for obstructed blood vessels far from the body's outer surface.

While directed drug transport to the thrombus site is of significant advantage, rapid thrombus dissolution is also hindered by penetration of fibrinolytic agents into the fibrin network. To overcome this limitation, an approach that enhances μwheel penetration into the fibrin network once it is delivered is required. Here we recognize that, driven by an applied external rotating field, μwheel torques are significant and can be used to impose mechanical forces on thrombi. To exploit these forces, we take inspiration from nature and the enhanced transport one can achieve through viscous or solid materials with motions and geometries that are not straight but rather helical in form. Specifically, corkscrew shapes and motions are effective in applications both at microscopic and macroscopic length scales. For example, at the microscale where viscous forces dominate fluid dynamics, bacterial swimmers have only two approaches available for translation, either corkscrew or flexible flagellar motion.[24] As a result, bacteria such as the genus *Spiroplasma*[25] with helical morphology use a corkscrew motion to swim.[26,27] At macroscales, corkscrew geometries are used to improve penetration, ranging from the well-known wine bottle opener to even larger scale augers and mixers. In fact, one mechanical thrombectomy device, the MERCI retriever, uses a corkscrew to remove thrombi from large arteries.[28] All of these tools take advantage of a corkscrew geometry's unique ability to bore into a denser or more viscous phase.

We take advantage of the enhanced penetration such a motion can create using the unique ability to quickly and precisely redirect rotating μwheels. With directional control performed through a simple shift in the applied field phase angle, we can create arbitrary translation patterns without increase in field strength or experimental complexity. Here and to demonstrate this approach, we functionalize μwheels with tPA and use them to lyse fibrin gels. Compared to soluble tPA that lyses at the gel surface, tPA-μwheels undergoing a corkscrew motion penetrate into the gel leading to a combined surface and bulk degradation that results in faster lysis. This biomechanical mechanism overcomes diffusion limitations associated with soluble tPA and provides physical action to disrupt gel structure.

2. Results and Discussion

μWheels were assembled and translated using magnetic fields of magnitude 9 mT rotating at frequencies of 100 Hz oriented away from a surface (**Figure 1**). A field vector that traces a circle yields a direct, straight-line motion (Figure 1A,D). A field vector that traces a helical loop yields a corkscrew motion that still leads to net forward translation (Figure 1B,E). For the same field strength and rotation frequency the corkscrew motion has an approximately twofold slower linear translation velocity than direct motion (Video S1, Supporting Information, where specific field conditions and μwheel size lead to 2.8 vs 1.4 μm s^{-1}). Other complex paths are achievable by varying the phase angle of the z-component of the magnetic field (Figure 1C). We compare the dissolution rate of fibrin gels with and without platelets using these two motions for

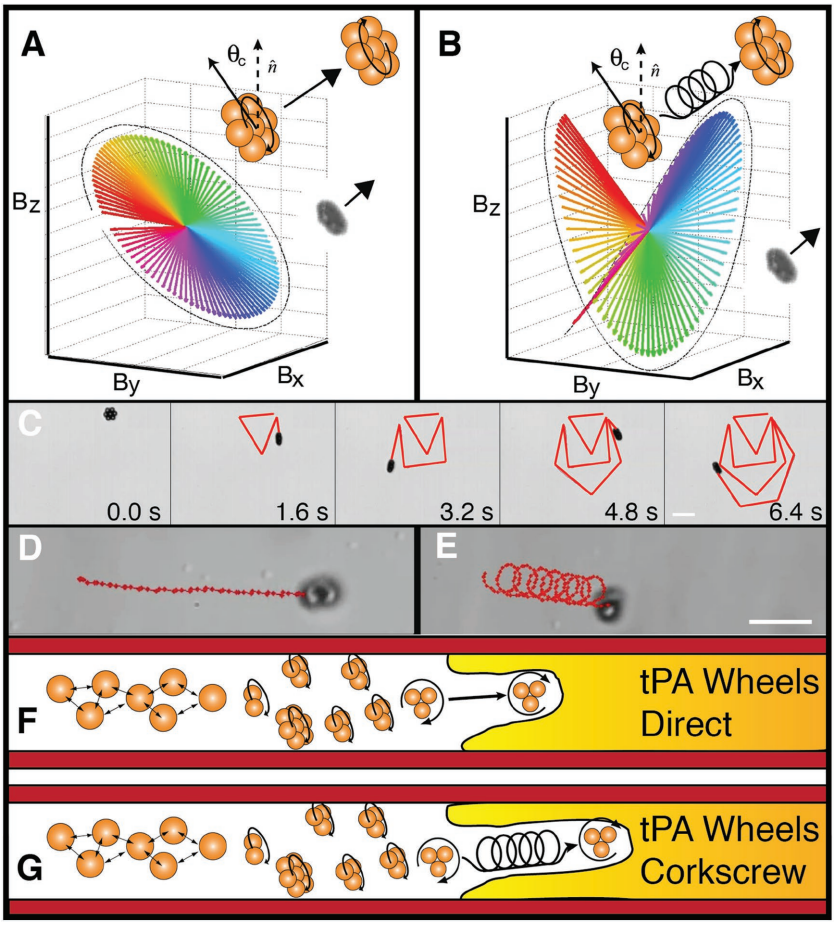

Figure 1. Approach to tPA-μwheel-induced reperfusion of occluded channels. A,C,D) With application of a rotating magnetic field, $\hat{B}$, oriented out of the surface plane at a camber angle θ_c relative to the normal $\hat{n}$, colloids assemble, "stand up," and roll along the surface. Color of vector tracing indicates field rotation angle. C) Because field orientation can be instantly changed, μwheels can be quickly redirected and follow preprogrammed or manually controlled paths. Scale bar = 10 μm. B,E) With a rotating "corkscrew" field, an additional helical component to wheel motion can be induced. Scale bar = 10 μm (Video S1, Supporting Information). While both modes can be used to assemble μwheels and do lead to high concentration of μwheels at the gel interface, F) direct motion based primarily on biochemical dissolution lyses slower than G) helical motion that yields combined mechanical and biochemical action.

μwheels functionalized with tPA and compare them to soluble tPA without μwheels (Figure 1F,G).

To first demonstrate enhanced transport down stagnant channels, we compare the delivery of tPA-functionalized μwheels (tPA-μwheels) to diffusion of tPA alone (**Figure 2**). Figure 2A shows the experimental geometry where tPA-coated beads were delivered into a stagnant channel, assembled within a rotating magnetic field into μwheels, and then translation velocities were directly measured. μWheels roll and accumulate at the interface of the fibrin gel (Figure 2A) where, consistent with our previous studies,[19] we observe a broad distribution of μwheel sizes (Figure 2B) and velocities (Figure 2C). With μwheels readily directed down stagnant channels in this manner, we compare tPA-μwheel drug delivery to free tPA diffusion. Using the measured velocity distribution (Figure 2C), we compare the concentration of tPA-μwheels at the gel interface to that of free tPA. In both cases, tPA is introduced at L = 1 mm distal of the gel interface at concentration, C_0. Upon field application, μwheels translate toward the fibrin gel front while free tPA diffuses. Comparing predicted concentration profiles at the gel surface in Figure 2D, two significant advantages are immediately apparent. The first is that the transit times of tPA to the interface are significantly decreased; importantly however and because transport is not driven by a concentration gradient, the local concentration of tPA on the μwheels at the gel is much higher than the initial concentration C_0. In contrast, for diffusive delivery of free tPA the concentration at the interface can only approach C_0. This accumulation of μwheels is readily observed experimentally as shown in Figure 2E and Video S2 (Supporting Information).

To demonstrate the relative lysing effectiveness of tPA-μwheels compared to soluble tPA, we form fibrin gels using thrombin and normal pooled plasma (NPP) with a height 70 μm and length 800 μm between two reservoirs of NPP in a microfluidic device (Figure 2A and illustrated in **Figure 3**A). Note that because all three compartments are filled with plasma or a plasma-derived fibrin gel, the endogenous inhibitors of tPA and plasmin, plasminogen activator inhibitor 1 (PAI-1) and α_2-antiplasmin, are present at physiologic concentrations. For quantification, the gel degradation front was monitored by optical microscopy as a function of time for two concentrations of tPA, 1 and 10 μg mL^{-1}, and two tPA-μwheel motions, direct and corkscrew (Figure 3B–D). Biotinylated tPA was immobilized on 1 μm streptavidin-coated superparamagnetic particles. These tPA-functionalized particles at a concentration of 1.5×10^6 μL^{-1} have a tPA mass concentration of 9 μg mL^{-1} and an activity of 930 IU mL^{-1}, which is comparable in activity to 3.6 μg mL^{-1} soluble tPA (Figure 3E). The roughly one-third reduced activity of the immobilized tPA compared to soluble tPA is expected because tPA molecules bind to particles in varying orientations, likely with some fraction bound with their enzymatic domains inaccessible to plasminogen. Note that we performed experiments both above and below the high end of systemic tPA concentration (≈3 μg mL^{-1}) following intravenous injection.[5]

For direct motion, a rotating magnetic field canted off the surface at 43° drives the assembly and translation of tPA-μwheels. Individual particles and small tPA-μwheels (2–7 particles) accumulate at the surface of the fibrin gel within the first 10 min and a small fraction of them penetrate into the fibrin gel (Video S2, Supporting Information). At late times (>20 min) however, μwheels become larger and larger,

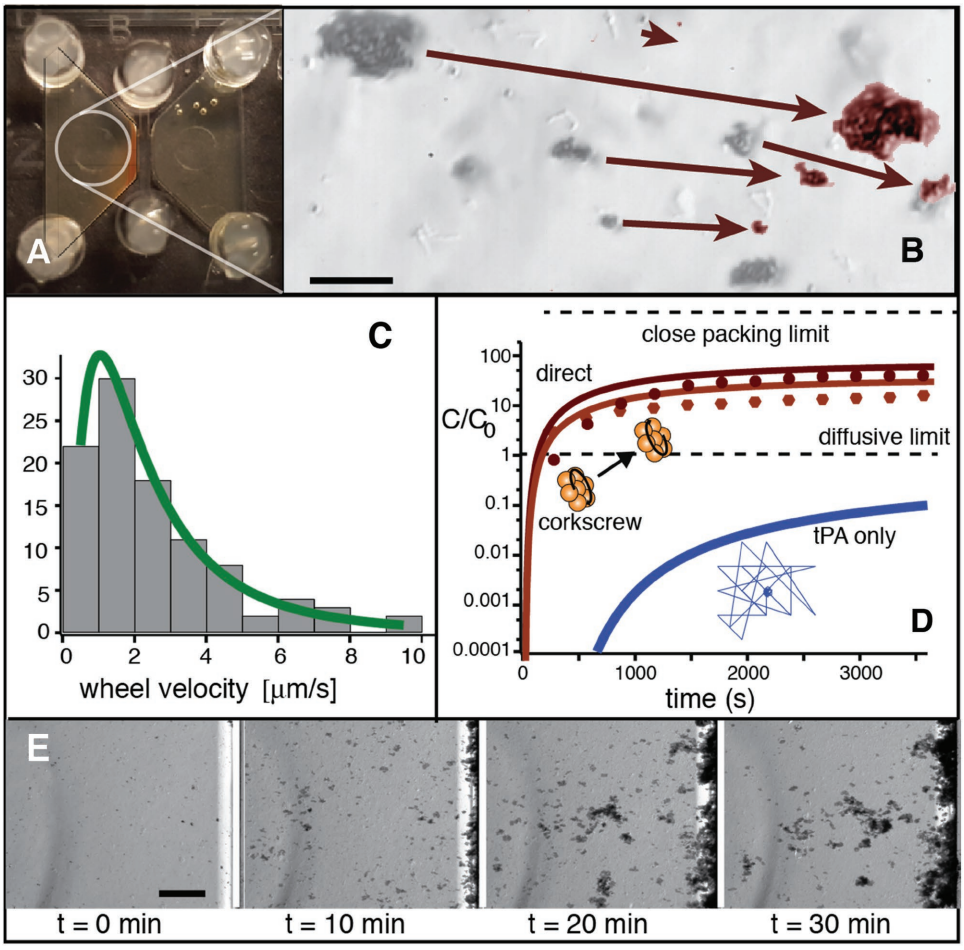

Figure 2. Wheel-based drug transport overcomes diffusion limitations down stagnant channels. A) Upon application of the magnetic field, tPA-μwheels accumulate at the front edge of the fibrin gel in a microfluidic device (rust colored region). Note the fibrin gel is present in the region separating the two reservoirs (see also Figure 3A). B) Larger μwheels translate faster than smaller μwheels as shown in red overlay (Δt = 10 s, scale bar = 10 μm). C) Measured tPA-wheel velocity distribution for direct motion (N = 102) with log-normal fit. D) Predicted tPA concentration C/C_0 at the gel front for L = 1 mm and both free tPA and μwheel-bound tPA (see the Experimental Section). Corresponding measurements of μwheel concentration at the interface shown as data points. Note that μwheel concentration quickly exceeds the maximum concentration achievable via tPA diffusion alone. E) Driven by wheel rolling only, μwheel accumulation at the gel front (right) is easily observed at low resolution (Video S2, Supporting Information, scale bar = 200 μm).

growing to discs with diameters as large as 50–100 μm. These larger μwheels tend to attract smaller μwheels, resulting in a reduced number of penetrators. Also, because of continuous rotation in one direction, wheels tend to roll tangentially along the liquid–gel interface as opposed to digging into the network.

For corkscrew motion, we use identical magnetic field magnitudes and frequencies except now we alter the μwheel direction angle from –90° to +90° in 45° increments at 0.1 s time steps, achieving a net forward motion bias in the process (Video S1, Supporting Information). This corkscrew motion inhibits larger assemblies and maintains μwheel translation perpendicular to the liquid–gel interface. These features result in a higher number of penetrating μwheels for the corkscrew motion compared to the direct motion.

tPA-functionalized μwheels overcome transport limitations facing soluble PA in two ways. First, as shown in Figure 2, μwheels accumulate at high density at the fibrin gel front as the translation velocity to the interface is significantly faster than the fibrin gel degradation rate with and without platelets (4–13 μm min^{-1}) (Figure 3F, and Video S3, Supporting Information). As such, local concentration of tPA is orders of magnitude greater than the initial concentration. This is in contrast to soluble tPA where the initial and local concentrations are, at best, equal; however, in practice, local tPA concentration is likely lower because of its adsorption to fibrin and limitations inherent in diffusion down a stagnant channel.[29] Second, and what is particularly unique to this approach, is that μwheel motion can be directed to penetrate into the fibrin gel, effectively altering the mechanism of degradation.

To frame our interpretation of μwheel penetration and its effect of fibrinolysis, we appeal to the concepts of surface and bulk erosion used to describe polymer degradation,[30,31] often in the context of degradable drug delivery systems. Surface erosion refers to degradation at the liquid–solid interface, a diffusion-limited process that accurately describes the dissolution of fibrin gels by tPA in solution.[32] Bulk erosion

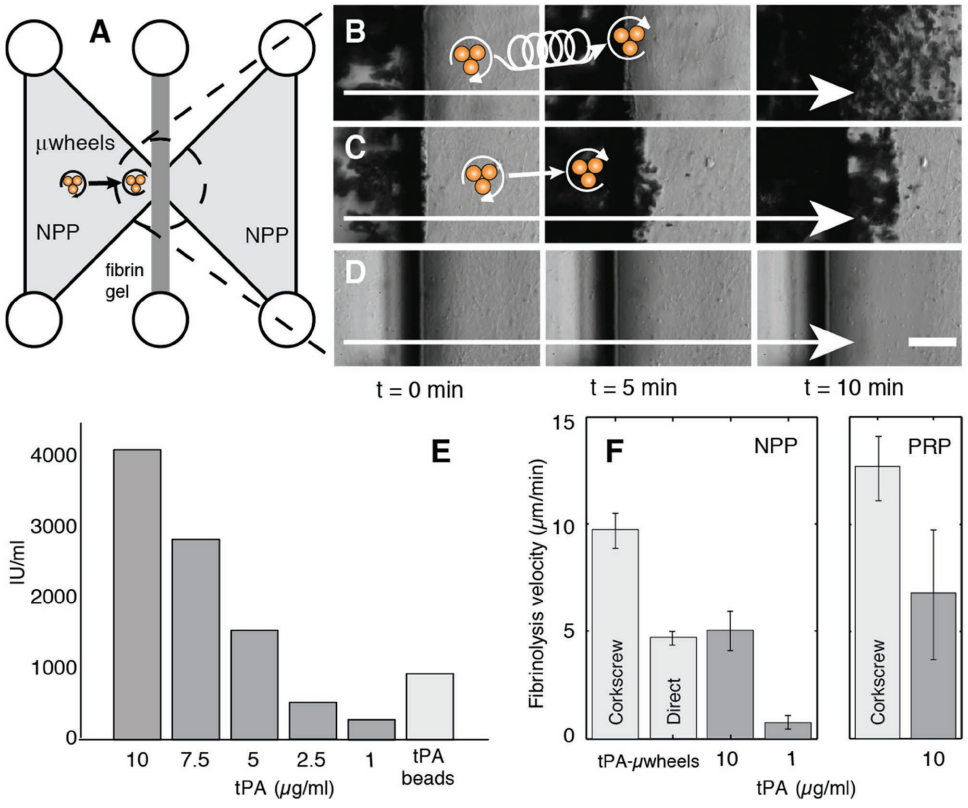

Figure 3. Faster lysis occurs with tPA-coated beads and addition of corkscrew action. A) Illustration of Figure 2A where a plasma-derived fibrin gel is formed between two normal pooled plasma (NPP) reservoirs. Images and data acquired near the center of the dashed circle region. B) tPA-coated beads (left) penetrating by corkscrew motion into fibrin gel, magnetic field strength = 9 mT, frequency = 100 Hz; C) tPA-coated beads and direct motion; D) soluble tPA alone (1 μg mL^{-1}), scale bar = 40 μm. E) tPA and tPA-coated bead activity measured by cleavage of a fluorogenic substrate. F) Fibrinolysis velocity of tPA versus tPA-μwheels for plasma-derived fibrin gels and gels formed with platelet rich plasma (PRP) (Video S3, Supporting Information).

refers to a homogenous inside-out degradation, a reaction-limited process when the transport into a solid matrix is faster than its degradation kinetics. In the case of soluble tPA, the process is dominated by surface erosion as the surface degradation kinetics are faster than diffusion of tPA into the fibrin gel. Our results suggest that this is indeed the case with average velocities of 0.81 ± .25 μm min^{-1} for the 1 μg mL^{-1} and 5.0 ± 1.5 μm min^{-1} for the 10 μg mL^{-1} tPA case. In experiments with tPA-μwheels however, fibrin dissolution shows significantly enhanced lysis velocities. We measured average velocities of 4.8 ± 0.3 μm min^{-1} for direct motion and 9.6 ± 1.5 μm min^{-1} for corkscrew motion into fibrin gels. Note, a fraction of penetrating tPA-μwheels translate at speeds faster than the degrading interface such that these lysis velocities underestimate the penetration velocity of some μwheels through the gel. With direct motion we observe degradation velocities comparable to concentrations at threefold the active tPA (10 μg mL^{-1}). For corkscrew motion, we see degradation velocities twofold faster than direct motion. For comparison, μwheels without immobilized tPA do not induce any lysis, suggesting that the mechanical forces imposed by the μwheels on the fibrin gel are not sufficient to rupture fibrin fibers. Similar enhancement in degradation rate with corkscrew motion is observed in fibrin gels derived from platelet-rich plasma (PRP, Figure 3F) and dense fibrin gels (NPP with 10 mg mL^{-1} fibrinogen, Figure S1, Supporting Information). For the dense fibrin gels, the corkscrew motion enhancement is ≈50% greater than direct motion. Here, because the gel pore size is comparable to the size of individual particles,[33] there is significantly less penetration than observed in NPP (Video S4, Supporting Information).

The biochemical mechanisms of fibrinolysis by tPA-functionalized μwheels may vary from soluble tPA. The rate of plasmin generation is enhanced by fibrin because tPA and plasminogen bind to it to form a ternary complex that promotes conformational changes and their interaction.[34,35] tPA and plasminogen can bind to fibrinogen and produce plasmin[36,37] but at a reduced rate compared to fibrin.[35] Degradation products including fibrin monomers and D-dimer can also bind tPA and plasminogen and accelerate plasmin generation to rates that are comparable to fibrin.[38,39] We hypothesize that initial fibrinolysis is mediated by a complex of immobilized tPA-fibrinogen-plasminogen, which may describe the lag time observed prior to observable movement of the fibrin interface (Video S3, Supporting Information). As degradation products are released and μwheels penetrate into the gel, the rate of fibrinolysis increases.

The combination of biochemical and mechanical action allows tPA-μwheels to penetrate into the gel, enhancing internal dissolution (**Figure 4**A–D) and increasing the velocity with which the surface front degrades. For direct motion, small μwheels (<4 particles) follow a relatively

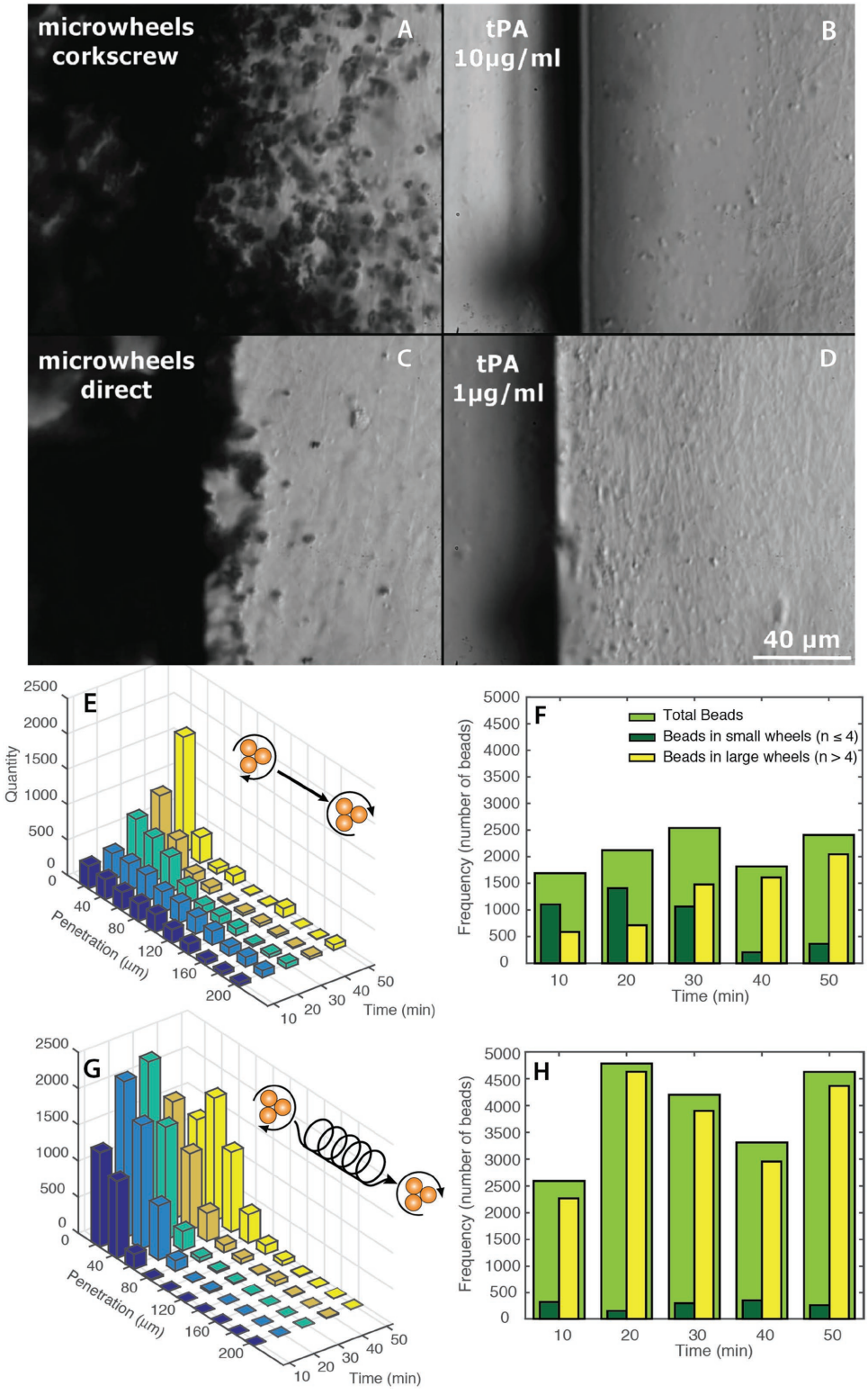

Figure 4. An increasing volume of tPA-μwheels penetrate into the gel as time proceeds via direct (biochemical) or corkscrew (biochemical + mechanical) lysis modes. A–D) Snapshot of Video S3 (Supporting Information) (t = 6 min) where improved penetration via corkscrew motion is apparent. E) Bead penetration with smaller wheels penetrating deeper. F) Penetrating beads with distribution of large and small wheels for direct motion. G) Corkscrew mode with higher total bead number penetration at shallower depth at short times. H) Penetrating bead distribution for corkscrew motion.

straight trajectory and penetrate 100–200 μm into the gel in the first 20 min of lysis (Figure 4E); however, after this initial transient, the size of penetrating μwheels increases and, accordingly the depth of penetration decreases. This is a result of large cluster formation at the front interface; big μwheels tend to grow at the expense of additional monomers

and smaller μwheels (Figure 4F). With introduction of a corkscrew motion, a near constant penetration depth of 40–60 μm was observed (Figure 2G). Here, penetrators are primarily larger μwheels (>4 particles) and more numerous. Unlike direct motion, corkscrew motion inhibits the formation of the largest assemblies (Video S3, Supporting Information). In addition, the helical pattern allows μwheels to sample the fibrin network and probe those weakest regions of the gel while direct motion μwheels are inhibited by relatively tough fibrin obstacles that are difficult to circumvent. These observations suggest that penetrating μwheels "soften" the gel by bulk erosion, which in turn results in faster front velocities.

To demonstrate that tPA-μwheels can also penetrate and degrade platelet-rich thrombi characteristic of arterial thrombosis and emboli, we turn to a previously developed microfluidic model of hemostasis.[40] In this model, collagen-mimetic peptides and tissue factor (TF) are adsorbed to the wall of a horizontal "injury" channel connected by two vertical channels (Figure S2, Supporting Information). One vertical channel is perfused with blood and the other with a wash buffer. To form a thrombus, blood is directed from the vertical blood channel into the injury channel under a constant pressure drop. Platelets and fibrin accumulate in the injury channel, forming an occlusive thrombus in ≈5 min. Following thrombus formation, we introduce tPA-μwheels into the wash channel and direct them into the thrombus using the corkscrew motion (Video S5, Supporting Information, and **Figure 5**). It takes ≈5 min for the first μwheels to penetrate through the thrombus along the wall of the injury channel. Over the next 25 min, much of the remaining fibrin is lysed and platelets are displaced as indicated by a reduced fluorescence intensity (Figure 5). These data show that tPA-μwheels can penetrate and lyse platelet-rich thrombi.

Experiments in this study using fibrin gels were performed in the absence of pressure gradients and thus any interstitial flow. These conditions are relevant both to deep vein thrombosis where fibrin-rich thrombi several centimeters in length can form, attenuating any pressure difference across the thrombus, as well as in to arterial thrombosis where low permeability platelet-rich thrombi result in very low interstitial flows even for significant pressure gradients.[33,41] In both cases, heterogeneities in thrombus structure can result in regions that are more permeable and more susceptible to fibrinolysis under pressure-driven flow.[42–44] In our studies, the size of individual colloids and small μwheels is on the same order of magnitude as dense fibrin gel pores[45] and may benefit from convective transport by either enhancing μwheel penetration or by conveying plasmin deeper into a thrombus.

With regards to potential biomedical application, we have observed that mechanical forces alone, without available tPA, are insufficient for gel lysis. This is expected as mechanical forces estimated from rotational frequency and wheel size based on fluid torque on a disk, $32\mu a^2\Omega/3$,[35] predict rotational forces of order pN. When one compares this value to the forces required to break up a fibrin network of order 1 mN,[46] it is clear that a biochemical component

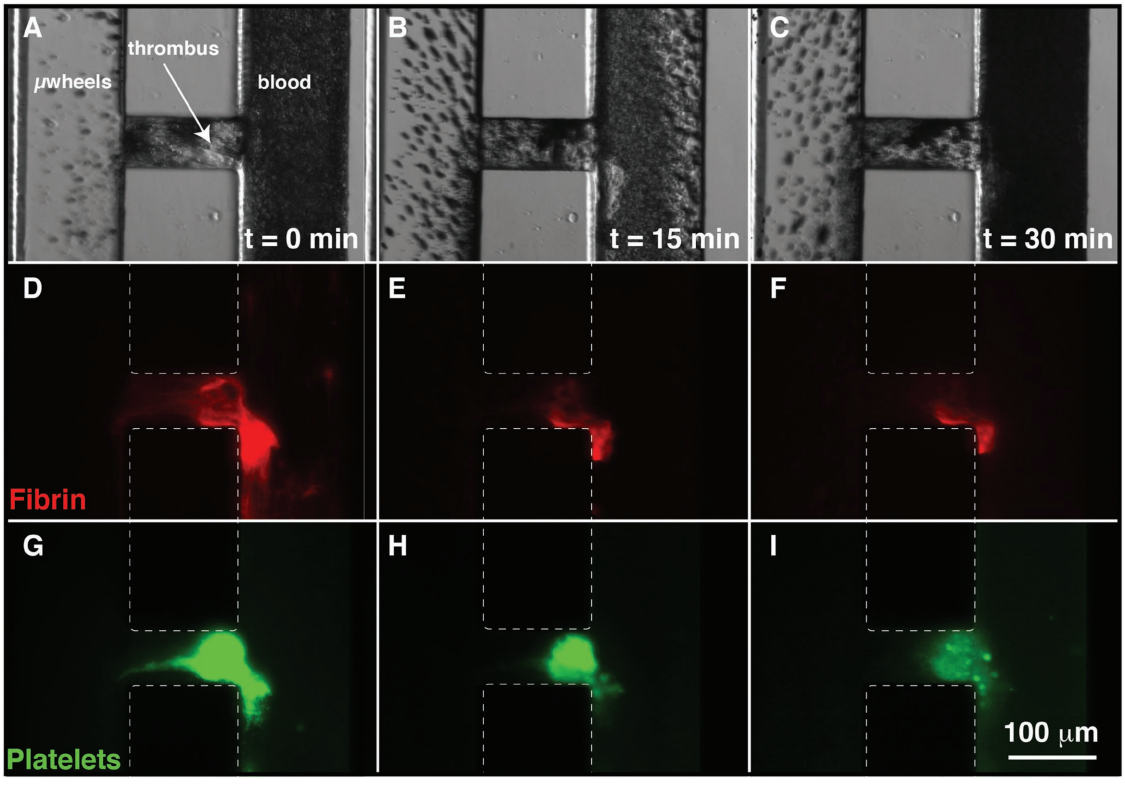

Figure 5. Fibrinolysis of a platelet-rich thrombus in a microfluidic model of hemostasis by tPA-μwheels. Snapshots from Video S5 (Supporting Information) at 0, 15, and 30 min. The thrombus occludes the horizontal channel coated with collagen-mimetic peptides and tissue factor. Following occlusion, μwheels are introduced from the left vertical channel with blood present in the right vertical channel. A–C) Brightfield images of μwheels accumulating at and penetrating into the thrombus. Epifluorescence of D–F) fibrin(ogen) and G–I) platelets.

is necessary for enhanced fibrinolysis. These relatively weak mechanical forces however, sufficient for μwheel transport, are an advantage for potential biomedical applications as 1 pN is insufficient to damage endothelial cells. In this, forces of 14.9 ± 1.6 nN μm^{-1} are required for cell rupture,[37] 3–4 orders of magnitude higher than the μwheel mechanical forces available here. In addition, and because the required field strengths are two to three orders of magnitude less than those required for MRI,[38] the surrounding physical infrastructure required is more readily achievable. The field magnitudes are not only significantly lower but also field gradients are not required to induce translational forces, a significant drawback associated with other magnetic-field-based microdevice manipulation approaches.[39]

There are several potential strategies for targeting occlusive thrombi in vivo that are compatible with the simple external magnetic fields required for rolling-based translation. If the approximate position of the thrombus is known, then the rotating field can be oriented to drive individual particles and assemblies in that general direction along vessel walls. This strategy would likely work best in occluded vessels where significant shear forces due to blood flow are not present. For particles and μwheels to escape from a vessel of normal or elevated blood flow into one with reduced or no blood flow, an additional gradient-based field may be required. Such magnetophoretic methods have had success in vivo to help guide catheters for treatment of brain diseases and stroke,[47] as well as to guide superparamagnetic particles toward occlusive thrombi.[16]

3. Conclusions

Biochemical dissolution of fibrin gels and thrombi by therapeutic concentrations of soluble tPA is a diffusion-limited process. Here, we show that a combined biochemical and mechanical lysis strategy can be implemented using directed assembly of colloidal μwheels functionalized with tPA. In this, dispersed colloidal particles are injected into the system at low density, assemble into μwheels in situ, and are then rapidly driven to the liquid–gel or liquid–thrombus interface creating a high local concentration of tPA. A unique feature of this approach is that tPA-μwheels not only accumulate at the surface but also are driven by a field that creates a corkscrew motion leading to penetration into the fibrin network or thrombus and bulk degradation which enhances surface dissolution. Because μwheels are approximately the same size as blood cells, they have potential application for relieving thrombosis in small vessels where catheters cannot reach and where systemic delivery of PA is ineffective due to transport limitations.

4. Experimental Section

Magnetic Field Setup: Magnetic fields were created using five air cored solenoid coils (50 mm inner diameter, 51 mm length, and 400 turns).[19] Applied voltages were generated using Matlab (Mathworks, Inc., Natick, MA) and an analog output card (National Instruments, NI-9263). Voltages from the output card were increased using three dual-output amplifiers (Behringer EP2000) before being applied to individual solenoids with currents monitored using an analog input card (National Instruments, NI-USB-6009). The total field strength at the center of the magnetic field system was up to 9 mT at 100 Hz (measured using a VGM Gaussmeter, Alphalab Inc.). For direct motion experiments, the magnetic field was programmed so that particles are constantly traveling in the +*x* direction (Video S1, Supporting Information). The corkscrew motion was programmed such that the particles traverse a forward biased spiral path where each cycle was completed in 1 s.

Wheel Assembly and Motion: Rotating magnetic fields were employed in-plane to assemble μwheels by isotropic interactions with size determined by local colloid concentration.[19] Spinning μwheels lying flat on a surface have no net motion; to roll, they must be inclined relative to the surface. To induce translation, a normal component was added to the magnetic field to reorient μwheels to a defined camber angle θ_c. Because rolling velocity is a balance of fluid drag and wet friction with the surface, important parameters are the number of particles comprising the μwheel and, as wheels rotate, the outer circumferential velocity. With this, we find rolling velocities up to and above 100 μm s^{-1} at field strengths of ≈15 mT with a scaling of $V \sim \omega n \cos(\theta_c)$ where ω is the angular frequency of the μwheel and n the number of particles in a wheel.

Preparation of tPA Conjugated Beads: Recombinant tissue plasminogen activator (Louisville APL Diagnostics, Inc., Seabrook, TX) was conjugated to biotin using N-hydroxysuccinimide (NHS) activated biotin (Life Technologies Corporation, Carlsbad, CA). Briefly, 50-fold molar excess NHS-biotin was allowed to react with tPA (200 μg mL^{-1}) over ice for 4 h. Excess biotin was removed using a desalting column (Life Technologies Corporation, Carlsbad, CA) with a molecular cutoff of 7000 Da. Biotinylated tPA (b-tPA) was stored in 20 μL aliquots at –80 °C until use. 5 μL of 1 μm streptavidin conjugated iron oxide beads (Thermo Fisher Dynabeads MyOne Streptavidin T1) were mixed with b-tPA (20 μL) and allowed to sit at 4 °C overnight to allow binding of b-tPA to the beads. Beads were then washed five times with 15 μL of 2% bovine serum albumin (BSA) in HEPES-buffered saline (HBS) to remove any unbound b-tPA.

Concentration Profiles: Predictions for the diffusion-driven time-dependent concentration of tPA down a stagnant channel were calculated from the 1D solution of Fick's law given a Heaviside step function initial condition and reflection at the fibrin gel boundary $z = L$. Following Crank, the following equation is obtained:[40]

$$\frac{C(z,t)}{C_0} = \frac{1}{2}\left[\operatorname{erfc}\left(\frac{z}{2\sqrt{Dt}}\right) + \operatorname{erfc}\left(\frac{2L-z}{2\sqrt{Dt}}\right)\right] \quad (1)$$

and, evaluating $C(z = L,t)$ with L = 1000 μm and D = 50 μm^2 s^{-1}, provides the time-dependent concentration $C(L,t)/C_0$ provided in Figure 2E. tPA-μwheel concentrations were predicted from the measured log normal velocity distribution (Figure 1C) and defined as:

$$f(v) = \frac{1}{v\sigma\sqrt{2\pi}} \exp\left[\frac{(\ln(v)-\mu)^2}{2\sigma^2}\right] \quad (2)$$

At a given distance z from the fibrin front, the probability p at time t of wheels reaching the front can be expressed as:

$$p(z,t) = 1 - \int_0^{z/t} f(v)\,dv = \frac{1}{2}\mathrm{erfc}\left[\frac{\ln\left(\frac{z}{t}\right) - \mu}{\sigma\sqrt{2}}\right] \quad (3)$$

Defining a wheel accumulation front width Δw = 100 μm allows expression of tPA-μwheel concentration at the fibrin interface (Figure 2E) as:

$$\frac{C(t)}{C_0} = \frac{1}{\Delta w}\int_L^{\infty} p(z,t)\,dz$$

$$= \frac{1}{2\Delta w}\left\{t\exp\left(\mu + \sigma^2/2\right)\mathrm{erfc}\left[\frac{\ln\left(\frac{L}{t}\right) - \mu - \sigma^2}{\sigma\sqrt{2}}\right] - L\,\mathrm{erfc}\left[\frac{\ln\left(\frac{L}{t}\right) - \mu}{\sigma\sqrt{2}}\right]\right\} \quad (4)$$

To compare to experimental values, beads (bulk concentration $C_0 = 1.5 \times 10^6$ μL^{-1}) were injected 1 cm from the front before being subjected to the rotating magnetic field. Once wheels reached within 1000 μm of the front, data collection was initiated and colloid flux into a control volume of width 100 μm from the front (height = 240 μm, depth = 70 μm) was quantified using ImageJ. Concentration of beads inside the control volume was determined by integrating the influx, assuming a negligible outflux as observed experimentally. Correspondingly for the theoretic curves of Figure 2D, limits of integration were set from L = 1000 μm to an upper limit of 10 000 μm. The close packed limit was determined by converting experimental values of C_0 to volume fraction and comparing to the hard-sphere random packing limit.[48]

Fibrinolysis Experiments: Fibrinolysis experiments were conducted using IBIDI μslide chemotaxis chips (IBIDI, Martinsried, Germany). These chips consist of one middle channel (6 μL) and two side channels (65 μL). To prepare fibrin gels, NPP was recalcified to $CaCl_2$ (20×10^{-3} M) and mixed with thrombin (final concentration 4.5×10^{-9} M), before being immediately injected into the observation channel of the chip. To make dense fibrin gels, exogenous human fibrinogen (Enzyme Research Laboratory, South Bend, IN) was added to the NPP to raise the final fibrinogen concentration to 10 μg mL^{-1}. After injection, the chip was kept in a humid box at room temperature for 1 h, then soluble tPA or the tPA-coated beads were injected in one of the side channels and the other side channel filled with NPP (George King Bio-Medical, Inc., Overland Park, KS). Each fibrinolysis experiment was conducted for 1 h and lysis was monitored and recorded using relief contrast microscopy on an inverted microscope (Olympus IX 70, 40× objective, NA 0.75) with camera (Epix SV 643M) operated at 30 frames s^{-1}. To maintain identical conditions between experiments, the magnetic field was applied both during tPA bead experiments and during soluble tPA experiments without beads as well. Solenoid coils were cooled with forced air with the temperature at the middle of the solenoids fixed at 26 °C.

tPA Activity Measurements: Activities of soluble tPA and tPA beads were determined using fluorescence measurements with a Biotek Synergy H1 Microplate Reader (BioTek U.S. Winooski, VT). Soluble tPA activities were determined for 1, 2.5, 5, 7.5, and 10 μg mL^{-1} tPA using a chromogenic substrate (100×10^{-6} M SN-18, Haematologic Technologies, Inc., Essex Junction, VT) in plasma in 20 μL working volumes. To obtain the tPA coated bead activity, beads were mixed with the substrate and NPP in 0.5 mL vials and then removed each hour using a permanent magnet to take a measurement.

Blood Collection and Preparation: Blood was collected from healthy donors by venipuncture into vacutainer tubes containing 3.2% sodium citrate. Donors had not consumed alcohol within 48 h prior to the blood draw, nor had they taken any prescription or over-the-counter drugs within the previous 10 d excluding oral contraception. The first tube of blood collected was discarded. All procedures were in accordance with the ethical standards of the responsible committee on human experimentation (University of Colorado, Boulder, CO) and with the Helsinki Declaration of 1975, as revised in 2000. Informed consent was obtained from all subjects for being included in the study. Aliquots of citrated 960 μL blood collected in sodium citrate were combined in tubes with 40 μL of Alexa-555 labeled fibrinogen (final concentration 56 μg mL^{-1}) which was added to visualize fibrin deposition. Platelets were labeled with the lipophilic dye DiOC6 (1×10^{-6} M final concentration). Labeled platelets were incubated at 37 °C for 15 min prior to the assay.

Microfluidic Model of Hemostasis: Platelet-rich thrombi were formed in a microfluidic model of hemostasis as previously reported (Figure S2, Supporting Information).[40] The master template for the device was prepared with photoresists (KMPR 1010 and KMPR 1050) to define a two-layer device with heights of 20 and 50 μm. Polydimethylsiloxane (PDMS) was molded off of these masters and covalently bonded to glass using standard soft lithography procedures. The device was designed in the shape of the letter "H" where the outer two vertical channels represent the vascular and extravascular compartments (10 mm long × 100 μm wide × 50 μm high), respectively. The vertical channels were connected by a horizontal channel (150 μm long × 50 μm wide × 20 μm high) representing a hole in the vessel wall, which is referred to as the injury channel. A mixture of three triple-helical collagen-mimetic peptides (100 μg mL^{-1}, Richard Farndale, University of Cambridge)[49]—a glycoprotein VI agonist collagen-related peptide (CRP-XL), the von Willebrand factor A3 domain binding site on collagen III (VWF-III), and a $\alpha_2\beta_1$ specific binding peptide (GFOGER)—was mixed 1:1 with tissue factor (TF, Dade Innovin) before being adsorbed to the walls of the injury channel at 4 °C for 12 h. The rest of the device was blocked for 1 h before the experiment with 2% BSA in HEPES buffered saline (HBS, 150×10^{-3} M NaCl, 25×10^{-3} M HEPES, pH 7.4). Pressure was controlled for the blood, recalcification buffer (75×10^{-3} M $CaCl_2$ and 35×10^{-3} M $MgCl_2$ in HBS), and wash buffer (3.2% sodium citrate in HBS) independently by applying a pressure to the headspace of their respective reservoirs using a pressure-based flow controller (Fluigent MFCS, Villejuif, France). Blood was recalcified in the ratio of 9:1 (citrated whole blood:recalcification buffer) using a herringbone mixer[50] to final concentrations of 7.5×10^{-3} M $CaCl_2$ and 3.75×10^{-3} M $MgCl_2$. The output from the herringbone mixer was connected to the blood channel of the extravascular injury device (Figure S2, Supporting Information). The pressures of the blood and recalcification reservoirs were held constant at 10 kPa. The pressure in the wash buffer was initially set to 3.5 kPa to drive a small amount of wash buffer through the injury channel while the blood channel was filled with recalcified blood driven by 10 kPa of pressure in the blood and recalcification reservoirs. The pressure

in the wash reservoir was then reduced to 1.75 kPa so that the blood passes from the blood channel into the injury channel and out into the extravascular channel. After the thrombus formed in the injury channel of the device, all external tubing was removed and tPA-functionalized beads suspended in 2% BSA in HBS were introduced into the extravascular wash channel with a number density of 1.5×10^6 beads μL^{-1} (effective tPA concentration: 3.6 μg mL^{-1}). The magnetic field was then used to induce corkscrew motion of the beads directed into the thrombus. Thrombus formation and lysis were monitored through an inverted microscope (Olympus, IX81, 20× objective, NA 0.45) equipped with a 16-bit CCD camera (ORCA-R2, Hamamatsu).

Statistical Analysis: Gel front positions were determined from stored video for all conditions investigated. With $N = 3$ measurements for separately prepared samples, averages and standard deviations were determined to perform a power law weighted least squares fit to $x = At^y$ using Igor Pro (Wavemetrics, Inc.). Errors reported to power law fits represent one standard deviation.

Supporting Information

Supporting Information is available from the Wiley Online Library or from the author.

Acknowledgements

T.O.T. and D.D. contributed equally to this work. The authors acknowledge support from the NSF (CAREER, CBET-1351672, KBN) and the NIH (R21NS082933).

Conflict of Interest

The authors declare no conflict of interest.

[1] C. Longstaff, K. Kolev, *J. Thromb. Haemostasis* **2015**, *13*, S98.
[2] J. W. Weisel, *J. Thromb. Haemostasis* **2007**, *5*, 116.
[3] L. A. Labiche, M. Malkoff, A. V. Alexandrov, *J. Neuroimaging* **2003**, *13*, 28.
[4] J. M. Gore, M. Sloan, T. R. Price, A. M. Randall, E. Bovill, D. Collen, S. Forman, G. L. Knatterud, G. Sopko, M. L. Terrin, *Circulation* **1991**, *83*, 448.
[5] S. L. Diamond, *Annu. Rev. Biomed. Eng.* **1999**, *1*, 427.
[6] S. Anand, J. H. Wu, S. L. Diamond, *Biotechnol. Bioeng.* **1995**, *48*, 89.
[7] A. C. Anselmo, C. L. Modery-Pawlowski, S. Menegatti, S. Kumar, D. R. Vogus, L. L. Tian, M. Chen, T. M. Squires, A. Sen Gupta, S. Mitragotri, *ACS Nano* **2014**, *8*, 11243.
[8] J.-C. Murciano, S. Medinilla, D. Eslin, E. Atochina, D. B. Cines, V. R. Muzykantov, *Nat. Biotechnol.* **2003**, *21*, 891.
[9] N. Korin, M. Kanapathipillai, B. D. Matthews, M. Crescente, A. Brill, T. Mammoto, K. Ghosh, S. Jurek, S. A. Bencherif, D. Bhatta, A. U. Coskun, C. L. Feldman, D. D. Wagner, D. E. Ingber, *Science* **2012**, *337*, 738.
[10] M. Shukla, U. D. S. Sekhon, V. Betapudi, W. Li, D. A. Hickman, C. L. Pawlowski, M. R. Dyer, M. D. Neal, K. R. McCrae, A. Sen Gupta, *J. Thromb. Haemostasis* **2017**, *15*, 375.
[11] S. Marinkovic, H. Gibo, M. Milisavljevic, M. Cetkovic, *Clin. Anat.* **2001**, *14*, 190.
[12] H. Chen, M. D. Kaminski, P. Pytel, L. Macdonald, A. J. Rosengart, *J. Drug Targeting* **2008**, *16*, 262.
[13] J.-P. Chen, P.-C. Yang, Y.-H. Ma, T. Wu, *Carbohydr. Polym.* **2011**, *84*, 364.
[14] A. J. Rosengart, H. Chen, Y. Xie, *Med. Hypotheses Res.* **2005**, *2*, 413.
[15] Y.-H. Ma, S.-Y. Wu, T. Wu, Y.-J. Chang, M.-Y. Hua, J.-P. Chen, *Biomaterials* **2009**, *30*, 3343.
[16] R. Cheng, W. Huang, L. Huang, B. Yang, L. Mao, K. Jin, Q. ZhuGe, Y. Zhao, *ACS Nano* **2014**, *8*, 7746.
[17] A. Blinc, C. W. Francis, J. L. Trudnowski, E. L. Carstensen, *Blood*, **1993**, *81*, 2636.
[18] I. N. Chernysh, C. E. Everbach, P. K. Purohit, J. W. Weisel, *J. Thromb. Haemostasis* **2015**, *13*, 601.
[19] T. O. Tasci, P. S. Herson, K. B. Neeves, D. W. M. Marr, *Nat. Commun.* **2016**, *7*, 10225.
[20] S. Bleil, D. W. M. Marr, C. Bechinger, *Appl. Phys. Lett.* **2006**, *88*, 263515.
[21] T. Sawetzki, S. Rahmouni, C. Bechinger, D. W. M. Marr, *Proc. Natl. Acad. Sci. USA* **2008**, *105*, 20141.
[22] P. Tierno, R. Muruganathan, T. M. Fischer, *Phys. Rev. Lett.* **2007**, *98*, 028301.
[23] A. C. H. Coughlan, M. A. Bevan, *Phys. Rev. E* **2016**, *94*, 042613.
[24] E. Purcell, *Am. J. Phys.* **1977**, *45*, 11.
[25] J. W. Shaevitz, J. Y. Lee, D. A. Fletcher, *Cell* **2005**, *122*, 941.
[26] B. Rodenborn, C.-H. Chen, H. L. Swinney, B. Liu, H. P. Zhang, *Proc. Natl. Acad. Sci. USA* **2013**, *110*, E338.
[27] B. Liu, M. Gulino, M. Morse, J. X. Tang, T. R. Powers, K. S. Breuer, *Proc. Natl. Acad. Sci. USA* **2014**, *111*, 11252.
[28] Y. P. Gobin, S. Starkman, G. R. Duckwiler, T. Grobelny, C. S. Kidwell, R. Jahan, J. Pile-Spellman, A. Segal, F. Vinuela, J. L. Saver, *Stroke* **2004**, *35*, 2848.
[29] J. P. Collet, D. Park, C. Lesty, J. Soria, C. Soria, G. Montalescot, J. W. Weisel, *Arterioscler., Thromb., Vasc. Biol.* **2000**, *20*, 1354.
[30] F. V. Burkersroda, L. Schedl, A. Göpferich, *Biomaterials* **2002**, *23*, 4221.
[31] S. Lyu, R. Sparer, D. Untereker, *J. Polym. Sci., Part B: Polym. Phys.* **2005**, *43*, 383.
[32] A. Blinc, C. W. Francis, *Thromb. Haemostasis* **1996**, *76*, 481.
[33] A. R. Wufsus, N. E. Macera, K. B. Neeves, *Biophys. J.* **2013**, *104*, 1812.
[34] L. Bányai, L. Patthy, *J. Biol. Chem.* **1984**, *259*, 6466.
[35] M. Hoylaerts, D. C. Rijken, H. R. Lijnen, D. Collen, *J. Biol. Chem.* **1982**, *257*, 2912.
[36] W. Nieuwenhuizen, A. Vermond, M. Voskuilen, D. W. Traas, J. H. Verheijen, *Biochim. Biophys. Acta, Protein Struct. Mol. Enzymol.* **1983**, *748*, 86.
[37] G. Tsurupa, L. Medved, *Biochemistry* **2001**, *40*, 801.
[38] J. H. Verheijen, W. Nieuwenhuizen, G. Wijngaards, *Thromb. Res.* **1982**, *27*, 377.
[39] J. H. Verheijen, W. Nieuwenhuizen, D. W. Traas, G. T. G. Chang, E. Hoegee, *Thromb. Res.* **1983**, *32*, 87.
[40] R. M. Schoeman, K. Rana, N. Danes, M. Lehmann, J. A. Di Paola, A. L. Fogelson, K. Leiderman, K. B. Neeves, *Cell. Mol. Bioeng.* **2017**, *10*, 3.
[41] R. S. Voronov, T. J. Stalker, L. F. Brass, S. L. Diamond, *Ann. Biomed. Eng.* **2013**, *41*, 1297.
[42] A. Zidansek, A. Blinc, G. Lahajnar, D. Keber, R. Blinc, *Biophys. J.* **1995**, *69*, 803.
[43] J. Vidmar, A. Blinc, E. Kralj, J. Balažic, F. Bajd, I. Sersa, *J. Magn. Reson. Imaging* **2011**, *34*, 1184.

[44] S. L. Diamond, S. Anand, *Biophys. J.* **1993**, *65*, 2622.
[45] A. R. Wufsus, K. Rana, A. Brown, J. R. Dorgan, M. W. Liberatore, K. B. Neeves, *Biophys. J.* **2015**, *108*, 173.
[46] M. Guthold, W. Liu, B. Stephens, S. T. Lord, R. R. Hantgan, D. A. Erie, R. M. Taylor, R. Superfine, *Biophys. J.* **2004**, *87*, 4226.
[47] C. Chautems, B. Zeydan, S. Charreyron, G. Chatzipirpiridis, S. Pané, B. J. Nelson, *Eur. J. Cardiothorac. Surg.* **2017**, *51*, 405.
[48] C. Song, P. Wang, H. A. Makse, *Nature* **2008**, *453*, 629.
[49] N. Pugh, A. M. C. Simpson, P. A. Smethurst, P. G. de Groot, N. Raynal, R. W. Farndale, *Blood*, **2010**, *115*, 5069.
[50] M. Lehmann, A. M. Wallbank, K. A. Dennis, A. R. Wufsus, K. M. Davis, K. Rana, K. B. Neeves, *Biomicrofluidics* **2015**, *9*, 064106.

Received: March 23, 2017
Revised: June 16, 2017
Published online: July 18, 2017

